AD-A172 993 A REVIEW OF AERODYNAMIC CHARACTERISTICS FOR SEVERAL RECOVERY SCHEMES OF REENTRY VEHICLES(U) FOREIGN TECHNOLOGY DIV WRIGHT-PATTERSON AFB OH Z HUANG 1/1

UNCLASSIFIED 18 SEP 86 FTD-ID(RS)T-0733-86 F/G 22/3 NL

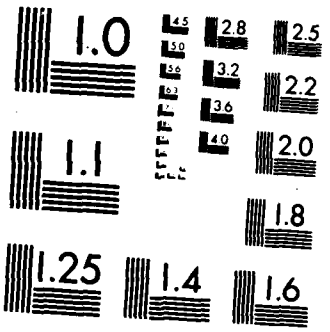

FTD-ID(RS)T-0733-86

AD-A172 993

FOREIGN TECHNOLOGY DIVISION

A REVIEW OF AERODYNAMIC CHARACTERISTICS FOR SEVERAL RECOVERY SCHEMES OF REENTRY VEHICLES

by

Huang Zhicheng

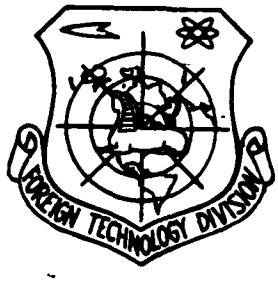

Approved for public release;
Distribution unlimited.

HUMAN TRANSLATION

FTD-ID(RS)T-0733-86 18 September 1986

MICROFICHE NR: FTD-86-C-002210

A REVIEW OF AERODYNAMIC CHARACTERISTICS FOR SEVERAL RECOVERY SCHEMES OF REENTRY VEHICLES

By: Huang Zhicheng

English pages: 26

Source: Kongqidonglixue Xuebao, Vol. 4, Nr. 1, March 1986, pp. 88-98

Country of origin: China
Translated by: FLS, INC.
F33657-85-D-2079
Requester: FTD/SDBS

PREPARED BY:

TRANSLATION DIVISION
FOREIGN TECHNOLOGY DIVISION
WPAFB, OHIO.

GRAPHICS DISCLAIMER

All figures, graphics, tables, equations, etc. merged into this translation were extracted from the best quality copy available.

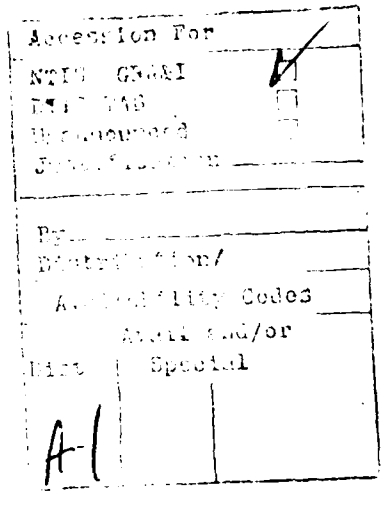

A REVIEW OF AERODYNAMIC CHARACTERISTICS FOR SEVERAL RECOVERY SCHEMES OF REENTRY VEHICLES

Huang Zhicheng
(China Aerodynamic Research and Development Center)

Abstract This paper conducts analysis and comparison of the aerodynamic characteristics for several recovery schemes of reentry vehicles. These schemes include the aft jettison mass plus parachutes, the sidewise jettison mass-drag cones plus parachutes, the towed cones plus parachutes, the drag brakes plus parachutes, and the aft jettison mass-drag brakes plus parachutes. The features of pattern of air flow for these schemes, the results of wind tunnel tests and the results of engineering calculation are emphasized. Based on this, a ballistic analysis and performance comparison for these schemes are carried out, and suggestions for the selection of schemes and further work are proposed.

This paper was received on Jaunary 11, 1985. A revised version was received on March 3.

I. Preface

For a long time, the recovery of reentry vehicles in one of the key technologies in the development of advanced reentry vehicles. The purpose for recovery in early days was to determine the survivability of a warhead in the reentry environment and the safety margin of the heat resistance design, and to certify the heat resistance design of the antenna window and the tip, large area heat shield. In recent years, however, the interest has shifted to the shape of corrosive combustion, factors that affect the rolling moment and the nonuniform corrosive combustion. The shape of low altitude corrosive combustion of recovery can provide basis for the study of effects of corrosive combustion on aerodynamics. It can also conduct overall evaluation of the theory of corrosive combustion and the performance of isntrument for testing the rate of indentation at the tip. In order to accomplish the above purposes of recovery, the ballistic coefficients after the appearance of maximum aerodynamic thermal environment must be decreased to 1/2 to 1/3 or their original values. At this time, the shape of the tip recovered will resemble the shape landed from real flight.

To jettison mass and to take measures that increases drag are the two basic methods of the recovery technology. They can be adopted separately or jointly to achieve the purposes of recovery. For increasing the drag, in addition to increasing the drag coefficient, it can also be achieved by increasing the bottom surface area. Since the bottom surface area often changes while mass is being jettisoned, this point should be noted when company the slowdown feature of each

scheme. To summarize from references abroad, the schemes which have already been studied for reentry vehicles with high ballistic coefficients are: (1) the aft jettison mass plus parachutes scheme[2]; (2) the sidewise jettison mass-drag cones plus parachutes scheme[3,4]; (3) the towed devices plus parachutes scheme[5-7]; (4) the drag brakes plus parachutes scheme[1,7,8]; (5) aft jettison mass-drag brakes plus parachutes scheme[1]; (6) control of attack angle scheme[9,10]. The last scheme is still in the research stage[34] because of its large lateral overload. This paper primarily discusses the first five schemes. The aerodynamic problems of scheme (1) is primarily the aerodynamic problems of the aft jettison mass. Scheme (5) is the combination of schemes (1) and (4). Thus, only schemes (2), (3) and (4) are discussed in terms of aerodynamics. The aerodynamic problems of these schemes, except for the problems of aerodynamic features and kinetics for more matured parachutes, require solution of problems in two areas: 1. the aerodynamic, aerodynamic thermal and kinetic problems of the recovered body. When comparing the schemes, mainly the drag features of each scheme are discussed and the static stability (in general, static stability will be increased when measures for increasing drag are taken) and the aerodynamic thermal environment are properly noted. 2. the aerodynamic problems during the process of jettisoning mass. The aerodynamic problems of the aft jettison mass are very close to those of jettison process of the towed cones. For the sidewise jettison mass, the aerodynamic interference problems of the shell body and the recovered body must be resolved in order to prevent collision of the two bodies and too much disturbance on the recovered body[11].

II. Discussion On The Separation Flow Of The Recovered Body

For the three schemes of sidewise jettison mass-drag cones, the towed cones and drag brakes, although the recovered body each has its features in the pattern of air flow, there do exist common rules between them, i.e., there are open and closed types of separation flow. This flow phenomenon was pointed out by Reference [12] when studying the supersonic air flow pattern around a hollow cave (Fig.1). For flow between the front and aft bodies, Reference [12] also pointed out that there was a critical value for the distance between the front and aft bodies, and that when this value was exceeded, there would be a closed trail, and an open trail when the distance was smaller than this value (Fig.2). It was also pointed out that when the ratio of the diameters of the front and aft bodies were close to 1, this critical value was the distance from the bottom of the front body to a point two to three front body diameters away. The air flow pattern of the recovered body in a specific scheme is much more complicated than those analyzed above. For the sidewise jettison mass-drag cones, though there are closed trails formed at the bottom of the front cone, attached flow or separation flow might appear in front of the skirt. For separation flow, there can be reattch or no reattach at the skirt depending upon different M number, Re number and shape of skirt, i.e., closed or open types of separation flow can be formed (Fig.3). Qualitatively speaking, when the skirt angle is too large (e.g., larger than 30°), or there is aft, steps with a large angle, and as the Re number decreases, separation flow is more easily formed. For the towed cones shceme, a single towed cone in a uniform incoming flow will also display attached flow and open type

separation flow (Fig.4). Yet under normal conditions, open type separation flows are more easily formed in the tail flow of the front body. If there is no rod or rope connecting the front and aft bodies (equivalent to the aft jettison mass), generally a detached shock wave will form in front of the towed cone, and the drag of the towed cone is larger (Fig. 2b). If there is a rod or rope connected, the air flow pattern is similar to that of the sidewise jettison mass-drag cones, and the open type separation flow formed at this time decreases the drag. The drag brakes scheme can be considered as a skirt with crevices, which is conducive to the formation of attached flow or closed separation flow. But for a small bluntness ratio and medium drag brakes angle, open type separation flows were observed in a wind tunnel experiment (Fig.5). The wind tunnel experiment has shown that if open type separation flow occurs on a recovered body, the drag decreases markedly; therefore, measures should be taken in the design to keep this type of flow from occurring.

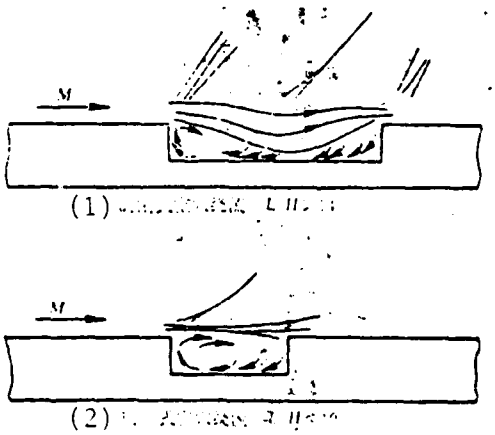

Fig. 1. Hollow cave air flow pattern
Key: (1) a. closed type hollow cave air flow pattern L/H 14;
(2) b. open type hollow cave air flow pattern L/H 10.

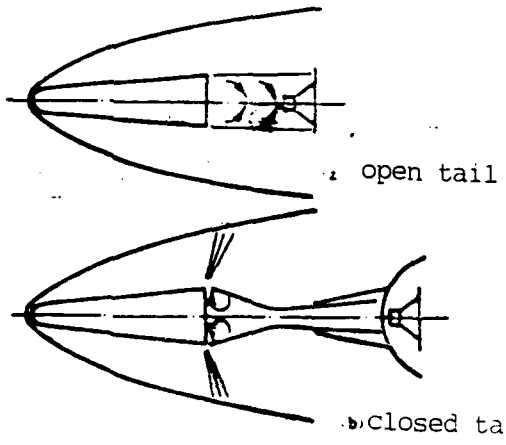

Fig. 2. Towed cones air flow pattern

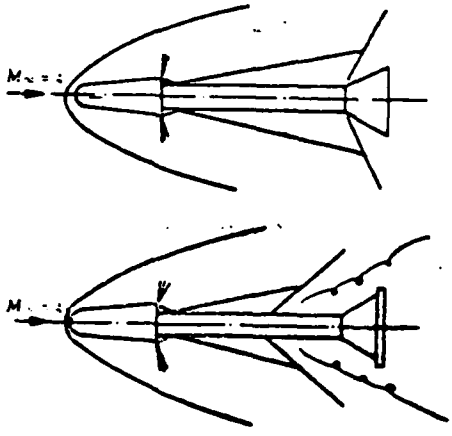

Fig. 3. Air flow pattern of sidewise mass-drag cones in high supersonic wind tunnel

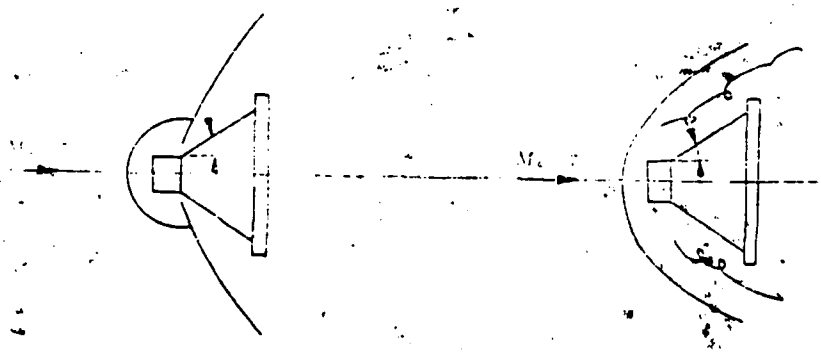

Fig. 4. Air flow pattern of single towed cones in high supersonic wind tunnel

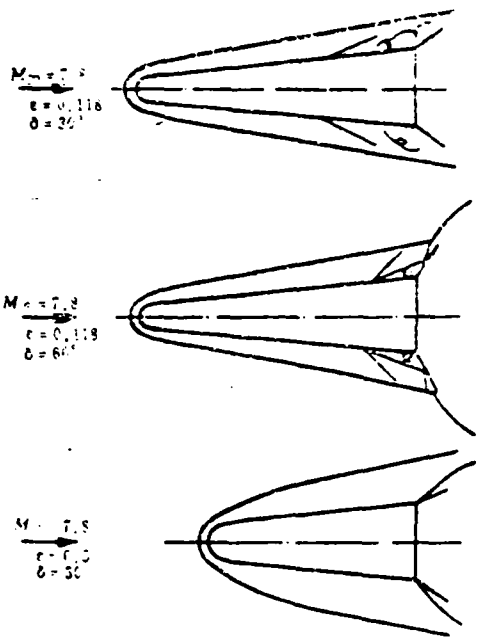

Fig. 5. Air flow pattern of drag brakes scheme in cannon wind tunnel

III. The Aerodynamic Features Of Sidewise Mass-Drag Cones Scheme

At M_∞=3.01, 4.02 and 5.05, the wind tunnel experiment[3] has shown that the drag skirts scheme is aerodynamically superior to the drag cone scheme with the center portion of the rod indented. The drag cone scheme tends to form a separation flow, while as long as the skirt angle is less than 30°, the drag skirt scheme can prevent the open type separation flow from occurring; the change of drag with respect to the shape of corrosive combustion and bluntness ratio for the drag skirts scheme is much smaller than that of the drag cones scheme. The pressure center for drag skirts is located farther behind than that of the drag cones. Due to structural reasons, only drag cones with a slight indentation can be manufactured in actuality and their aerodynamic features should be close to those of the drag skirts.

Through tests in a transonic wind tunnel[10], high supersonic wind tunnel[14] cannon wind tunnel[15] shock wave wind tunnel[15,16] and free flight ballistic target[17], the results are as follows:

1. The shape of the drag cone has obvious effects on drag. In the high supersonic wind tunnel, the drag of shapes with aft cone angles of 25° and 40° are all smaller than that of a shape with an aft cone angle of 30°. If the drag cones have aft steps, the drag is lowered. At M_{∞}=4.04 and an aft cone angle of 30°, after the aft steps are removed, the drag coefficient increases from 0.26 to about 0.60; but at an aft cone angle of 40°, after the aft steps are removed, the drag coefficient only increases from 0.25 to 0.29. When the aft cone angle equals 30°, the drag cone becomes four swept-back wings and the drag coefficient reaches 0.54.

2. The changes of the bluntness ratio and the shape of corrosive combustion have great influences on the drag. The results of tests in the cannon wind tunnel and shock wave wind tunnel have shown (Fig. 6) that the drag coefficient lowers as the bluntness ratio increases. The effects of shapes on corrosive combustion were also tested in the cannon wind tunnel (including indented shape, 55° double-cone shape and flat-head shape), and all these shapes caused the drag coefficient to drop with the most caused by the double-cone shape, 9%.

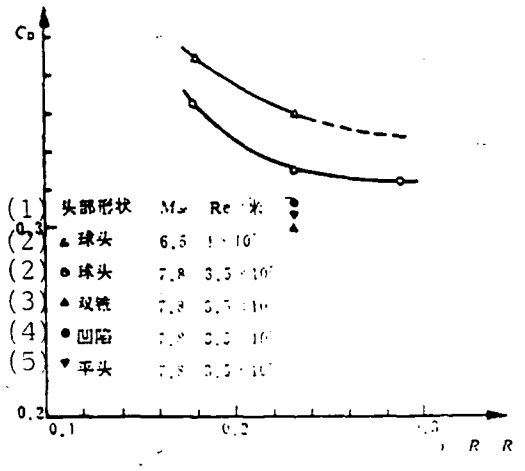

Fig. 6. The change of drag coefficient at zero attack angle with respect to bluntness ratio for the recovered body of the sidewise jettison-drag cone scheme.
Key: (1) Head shape; (2) spherical head; (3) double-cone; (4) indented; (5) flat-head.

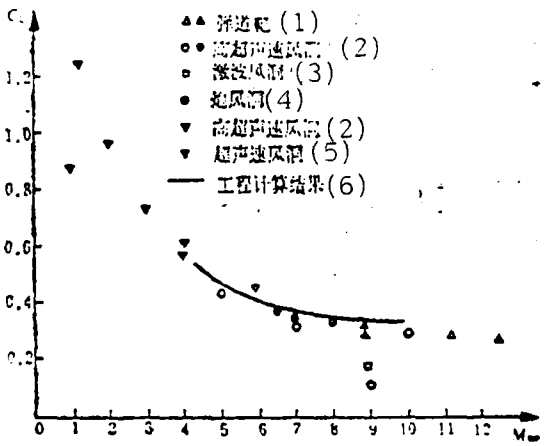

Fig. 7. The change of drag coefficient at zero attack angle with respect to M_∞ for the recovered body of the sidewise jettison-drag cone scheme.
Key: (1) ballistic target; (2) High supersonic wind tunnel; (3) shock wave wind tunnel; (4) cannon wind tunnel; (5) supersonic wind tunnel calculation; (6) engineering calculation results.

3. The results of tests in wind tunnels with different range of M_∞ number and those of the free flight ballistic target tests can be connected (Fig. 7). Figure 7 also lists the results from engineering calculations. The pressure distributions of front and aft cones were

calculated by using the internal Newton theory. The parameters at the outer portion of the boundary layer underwent the entropy layer swallowing process and by using the commonly used heat flow formula through the Reynold simulation to back calculate the frictional drag. The pressure at the bottom was calculated using the common experience formula from references. The calculated results have shown that for cases without open type separation the calculations are in fair agreement with results from various testing devices. The results from high supersonic wind tunnel with $M_\infty=7$, $P_o=29$ atmospheric pressures was slightly lower ($C_D=0.305$); at $P_o=68$ atmospheric pressures, C_D increased ($C_D=0.329$, represented by black dots in the figure) and the flow field photographs verified that it was attached flow. The result for said wind tunnel with $M_\infty=9$, $P_o=60$ atmospheric pressures was lowered more ($C_D=0.145$) and from the flow field photographs it could be determined that open type separation flow had occurred. Figure 8 shows the change of axial drag coefficient with respect to attack angle. At $M_\infty=9$, the axial drag coefficient increases rapidly as increases, and this indicates that as the attack angle increases attached shock waves formed on the skirt surface facing the incoming air flow. While at $M_\infty=5$ and zero attack angle, attached shock waves formed in front of the skirt; therefore, the change of axial drag coefficient with respect to attack angle was not as abrupt. For the free flight experiment in the shock wave wind tunnel, at $M_\infty=8.9$, the drag coefficient was about 0.18 and $Re=1.3 \times 10^6/m$. For the experiment in the transonic wind tunnel, at $M_\infty=1.15$, the drag coefficients were lowered more and from the flow field photographs, it could be seen that open type separation flow was present. It should be noted that there was a slight difference in scale between the model original-

ly used for free flight ballistic target experiment and that of the high supersonic wind tunnel experiment. Experiments using identical models were conducted later and the drag coefficients obtained were slightly lower (represented by black dots in the figure). The silhouette photographs of the free flight ballistic target verified that shock waves were present at the skirt.

4. In all the experiments, no matter how the shape changes, the ratio of the location of the pressure center to the length of model is greater than 0.8 within the wide M number and attack angle change range. Therefore, if the center of gravity is properly placed, greater margin of static stability can be obtained.

5. The results of free flight ballistic target have shown that $C_{m_g}+C_{m_{\dot{\alpha}}}$ is positive and its value is between 1 and 3. The results from the internal Newton theory[18] also indicate that, when the attack angle is smaller than 4°, $C_{m_g}+C_{m_{\dot{\alpha}}}$ is also positive; therefore, under a small attack angle, negative damping situations could occur.

In addition to drag measurement experiments, pressure measurement experiments were also conducted for the recovered body in the high supersonic wind tunnel[19], and heat flow and pressure distribution measurements were conducted in the shock wave wind tunnel. The results of experiments show that: the pressure and heat flow values on the rod section were lower and their changes smoother. At the skirt, the results for high supersonic wind tunnel at $M_{\infty}=5$ and with pointed head or small bluntness ratio, a peak value for pressure occurs. When bluntness ratio is larger, the pressure increases nonlinearly; while

under larger M number in the shock wave wind tunnel, peak value occurs for both pressure and heat flow with the location of peak heat flow value closer to the front than that of the peak pressure value, but the maximum heat flow value did not exceed half of that at the resident point. The comparison of the results of our heat flow engineering calculations and the experiments shows that, except for the calculated values in a small section behind the aft steps being a little high, the rest of the sections were in fair agreement (Fig. 9). Since the effects of aft steps were omitted during calculation, the discrepancy near the aft steps was predictable.

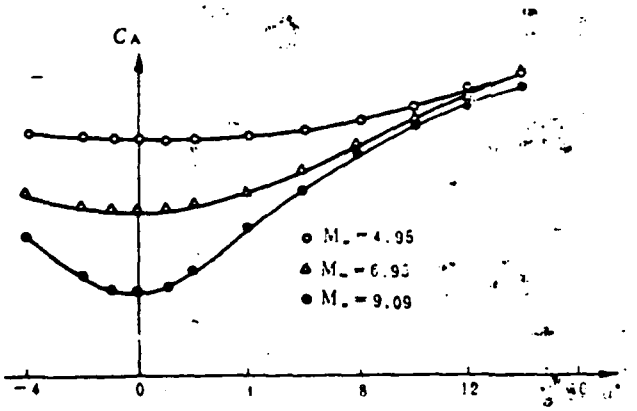

Fig. 8. The change of axial drag coefficient with respect to attack angle for a recovered body of the sidewise jettison-drag cone scheme in the high supersonic wind tunnel.

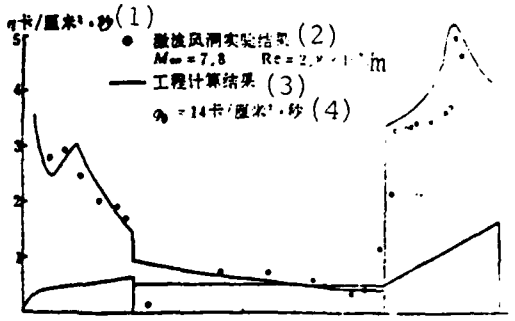

Fig. 9. Heat flow distribution for the recovered body of the sidewise jettison-drag cones scheme

Key: (1) q cal/cm^2.sec; (2) shock wave wind tunnel experiment results; (3) engineering calculation results; (4) 14 cal/cm^2.sec.

IV. The Aerodynamic Features Of The Towed Cones Scheme

Towed cone is the most typical among towed devices. The towed cone can be rigidly connected or flexibly connected to the recovered body. For the aerodynamic features of the towed cone, the most interesting ones are the problems of towed cone drag and stability. Experiment results from abroad[5,6] show that the front body is always a pointed cone and the M numbers during experiment are lower. Through the drag measurement experiments conducted in a transonic wind tunnel[19] and high supersonic wind tunnel[20, 21], the following results are obtained:

1. The experiments verified the concept of "critical distance." The experiments have shown that: the critical distance is less than 3 times the bottom diameter of the front body. The experiments also verified that the critical distance moves closer to the front when the towed cone is moved forward than when it is moved backward.

2. The experiments have shown that the front body's bluntness and the tip's shape of corrosive combustion have obvious effects on the drag of towed cone. The larger the bluntness, the smaller the drag of towed cone (Fig. 10). When the bluntness ratio is 0.461 and the tip is changed to 55° double-cone, C_D decreases by 10%. The drag coefficient decreases faster as the M number increases (Fig. 11).

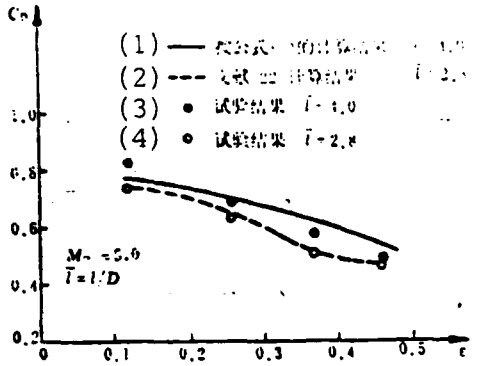

Fig. 10. The change of drag coefficient with respect to bluntness ratio for towed cones in the high supersonic wind tunnel
Key: (1) calculated results according to formula (1) $\bar{l}$=1.0; (2) calculated results from Reference 22 $\bar{l}$=2.8; (3) experiment results $\bar{l}$=4.0; (4) experiment results $\bar{l}$=2.8.

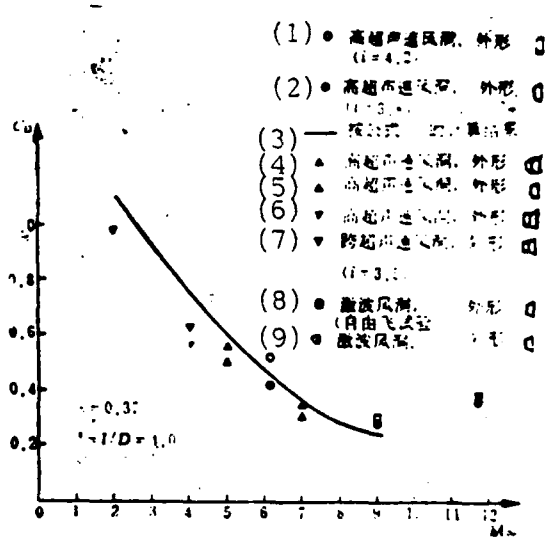

Fig. 11. The change of drag coefficient for towed cones with respect to M_∞.
Key: (1) High supersonic wind tunnel, shape; (2) High supersonic wind tunnel, shape; (3) Calculated results according to formula (1); (4) High supersonic wind tunnel, shape; (5) High supersonic wind tunnel, shape; (6) High supersonic wind tunnel, shape; (7) Transonic wind tunnel, shape; (8) Shock wave wind tunnel, shape (free flight experiment); (9) Shock wave wind tunnel, shape.

3. The experiments have shown that the drag coefficient in the tail flow field of the front body of the towed cones decreases as M increases. The difference of towed cones drag coefficient in uniform and nonuniform flow fields increases as M_∞ increases. In an uniform flow field, the towed cones drag coefficient at a cone angle of 40° is smaller than that of 30°. This is due to the presence of open type separation flow in the former (Fig. 4).

4. The Reynold number also has certain effects on the towed cone drag. In the high supersonic wind tunnel at $M_\infty=4$, when the pressure in the front chamber increases from 2.5 to 25 atmospheric pressures and the corresponding Reynold number increases from 0.116×10^8/m to 1.142×10^8/m, the drag coefficient increases by 10%.

5. The connecting rod and rope make the towed cone drag coefficient lower than without the rod and rope. It could been seen from the photographs that separation shock waves occurred on both the rod and rope thereby causing the drag coefficient to drop.

6. The shape of towed cones also has effects on the drag coefficient. In the high supersonic wind tunnel at $M_\infty=5$, when the front steps are removed, the drag coefficient increases from 0.457 to 0.50; when the aft brakes are removed, the drag coefficient drops to 0.43. When the cone angle of the towed cones is changed from 30° to 40°, the drag coefficient increases.

Reference [22] assumes that the location of the neck of trail is at twice the diameter of the bottom and that the width of the neck is

half of the diameter of the bottom. Using the line connecting the midpoints of the shoulder and neck as the border for circulation flow, then calculations are conducted according to methods in Reference [23]. The calculated distribution of kinetic pressure is in fair agreement with the experiment results of other countries. As the distance away from the bottom increases, the peak value of kinetic pressure increses, and the location of peak value deviate farther away from the axial line. This is caused by the shock waves at the neck. The calculated results also show that the bluntness ratio of the front body also has obvious influence on the cross-section of kinetic pressure. Peak value of kinetic pressure is small for large bluntness ratio and the location of peak value deviates farther from the axial line. Moreover, according to Reference [24], we believe that there is similarity in the velocity cross-sections of the trail often the critical distance. Combining the formulae in Reference [24, 25], along with the effects of M number, the correlation formulae of velocity cross-section are given as:

$$\frac{V}{V_\infty} = 1 - A\left(\frac{\bar{X}}{D}\right)^{-0.5} e^{B\left(\frac{Y}{D}\right)^2} \qquad (1)$$

$$A = 0.42\, e^{\left(6.21 M_\infty^{-\frac{1}{2}} C_D\right)} \qquad (2)$$

$$B = -7.89 C^{\left(-1.21 C_D\right)} \qquad (3)$$

where D is the bottom diameter of the front body, X is the axial distance measured from the bottom of the front body, Y is the vertical distance from the center axis and C_D is the drag coefficient. After the kinetic and velocity cross-sections are obtained, and based on Reference [26], the drag of towed cone can be calculated by using the modified Newton theory. It can be seen from Figs. 10 and 11 that better results were obtained from the above two methods.

The experiments[20, 21] on the stability of the towed cones in the high supersonic wind tunnel have shown that: there is unstable zone near the critical distance, which is consistent with the results in Reference [5, 6, 27]. These References also point out that unstable situation occurs when the half cone angle of the towed cone is increased to 45° or at a half cone angle of 40° but the brake diameter of the towed cone is 15% larger than that without the brake. Reference [35] conducted a preliminary aerodynamic analysis for the experiment results from the high supersonic wind tunnel.

V. The Aerodynamic Features Of The Drag Brakes Scheme

The drag brake is a drag-increasing measure commonly used on vehicles. Wind tunnel experiments have shown that: smaller wing surface displayed on the outer surface of a reentry vehicle can produce substantial drag. And the number, location, shape and size of the wing have obvious influences on drag. The scheme we studied was a reentry vehicle with four brakes extending from its bottom. Through testing in the high supersonic wind tunnel[28] and shock wave wind tunnel[29], the following results can be obtained:

1. Although there are great differences between the conditions of the high supersonic wind tunnel and the shock wave wind tunnel, the trends of the experiment results, however, are consistent. The drag-increasing effect of the drag brakes increases as the attack angle, bending angle and the ratio of drag brake area and bottom area increases; it decreases as the M number (when attack angle is small) increases. The advantages of the drag brake scheme when compared

with other schemes are larger drag coefficient even under high M number and relatively smooth changes with respect to M number under high M number.

2. The bluntness of the recovered body has obvious influence on the total drag. When there are no drag brakes the drag of the reentry vehicle increases as the bluntness ratio increases. However, the increase in bluntness ratio causes the M number in front of the drag brakes and the kinetic pressure to decrease; therefore, there is a critical bluntness ratio and the total drag thereof is a minimum (Fig. 12).

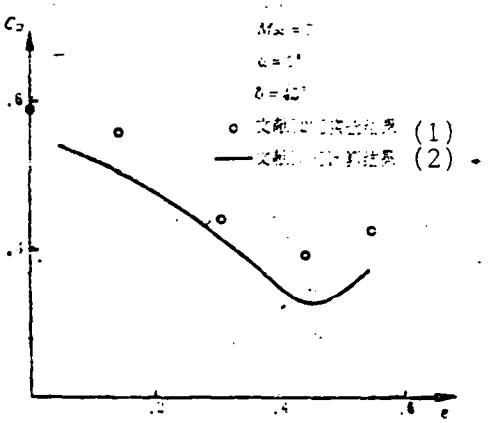

Fig. 12. The change of drag coefficient at $M_\infty = 7$ with respect to bluntness ratio for the drag brakes scheme.
Key: (1) experiment results from Reference [28]; (2) experiment results from Reference [30].

3. As the attack angle approaches 0° or at small attack angle, the drag-increasing effect is better when the height of the drag brake is increased rather than the width. At such time the proportion of increase in drag exceeds that of the drag brake surface area. This is due to the reason that the range of high pressure zone on the brakes is enlarged. For example, at $M_\infty = 7$, bluntness ration $\varepsilon = 0.259$,

and bending angle $\delta=45^{\circ}$, when the ratio of drag brake surface area to the bottom surface area increases from 0.048 to 0.064, the drag coefficient at zero attack angle increases from 0.3 to 0.437. But after the attack angle $\alpha \geqslant 4^{\circ}$, the effects of increasing the height of drag brake and increasing the bending angle are significantly reduced.

4. The change in the shape of corrosive combustion causes the drag coefficient to decrease markedly. When the head is a 55° cone and at $M_{\infty}=7$, the drag coefficient is reduced by 7%.

Reference [30] provided the engineering calculation methods for the aerodynamic features of the drag brake scheme. The influence of separation flow and entropy layer swallowing were considered in the calculations, and the M number and kinetic pressure in front of the brake were modified. But the three-dimensional effects of the drag brake and the influences of the nonuniform flow field in front of the brake were not taken into consideration. The calculated results of this method and the data from wind tunnel experiments were basically in good agreement (Fig. 12). For the high supersonic wind tunnel, the calculated critical bluntness ratio (about 0.38) and the experiment result was in fair agreement. Yet for the shock wave wind tunnel experiments, no critical bluntness ratio was found in the results.

Reference [31] studied the thermal environment of the drag brakes and the influences of the change in the shape of drag brake corrosive combustion on drag coefficient. When the bending angles are 45° and 60°, very high heat flow peak value occur on the brake and the shock wave wind tunnel experiments[32] verified this conclu-

sion. This might cause the drag brake surface facing the incoming air flow to be burned into a dented shape[33], thereby causing the drag coefficient to decrease more[31].

VI. Ballistic Analysis And Performance Comparison

We conducted the ballistic analysis and performance comparison of every scheme for a typical reentry vehicle. The geometrical dimensions of each scheme are limited by structure. The ratio of drag brake surface area to the bottom surface area for the drag brake scheme was selected as 0.064. The drag coefficients for every scheme were obtained by using the data from wind tunnel experiments after the smooth-out process along with the engineering calculation method to extrapolate to high M numbers (Fig. 13). The nonviscous drag coefficients of a reentry vehicle before recovery adapted the calculated results of the nonviscous data, and the frictional drag and bottom drag adopted the commonly used experience formulae. The ballistic calculation for each scheme was conducted on this basis. When conducting performance comparison, our interests are in: 1. if supersonic parachute is not used, decreasing the M number at the altitude of 2.5 kilometers to M_{∞}=1.0; 2. the touchdown velocity not exceeding 30 m/sec; 3. the changes of axial overload when the recovery altitude is reached; 4. the kinetic pressure when parachute opens which satisfies the demands for opening the parachute without causing damages[2]. The time for the towed cone to be towed out were set at 0, 0.5 and 1.0 second, respectively. Two ways for opening the drag brake were considered with the first way of opening it all the way to 54^{o} at once

and the second one of first opening it to 30°, then to 54° after 0.5 or 1.0 second.

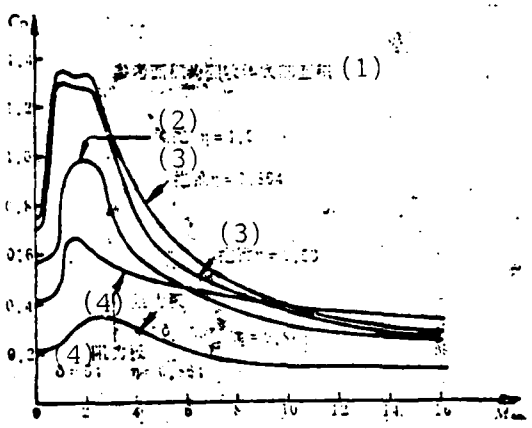

Fig. 13. The drag coefficients of ballistic analysis for each scheme. Key: (1) The reference surface area is the bottom surface area of the recovered body; (2) sidewise jettison; (3) towed cone; (4) drag brakes.

The calculated results have shown that: the aft jettison mass plus parachute scheme opens parachute at M_∞=2 after jettisoning 60% of the mass. The recovery altitude is set at 7 kilometers and the parachute drag coefficient is selected as 1.0, thus the demands for safe recovery are satisfied. When jettisoning, the maximum overload is only 142 grams. Therefore, this scheme has the advantages of being simple, reliable and with small overload. The key problem is whether the manufacturing and structure of the supersonic parachute allow it to jettison so much weight. For the towed cone scheme, let η be the ratio of the length of the recovered body to the length of the vehicle, and at η=0.864 and no jettison of mass, the demands are barely being satisfied only when recovery begins at 7 kilometers. The error in drag coefficient is considered, and only at η=1.0 (no jettison of

mass) can the demands be satisfied. If the structural design is such that the length of the recovered body decreases as weight is being jettisoned, then often due to too small a bottom surface area and an increase in the bluntness ratio, the increase in drag becomes insufficient. At η=0.53, even with 50% jettisoned weight the demands can still not be satisfied. Under a selected drag brake surface area, the demands for the drag brake scheme cannot be sa isfied without jettisoning weight. At η=0.864, the time interval between the two brake openings is 1.0 second, and at least 44% of the weight must be jettisoned in order to satisfy the demands. For the sidewise jettison-drag scheme, if the recovery altitude is set at 7 kilometers, the demands can be satisfied with just 30% of the weight jettisoned and still leaving plenty of margin. If 50% of the weight is jettisoned, the recovery altitude can be reduced to 4.5 kilometers. For a recovery altitude of 7 kilometers and 50% of weight jettisoned, the typical data for each scheme are listed in Table 1:

(1)方 案	(2)侧 抛	(3)拖 锥		(4)阻 力 板		
η	1.0	0.864		0.53	0.864	
Δt(秒)(5)	0	0	0.5	0	0	1.0
M_{max} 公里(6)	0.217	0.220	0.221	1.329	0.338	0.536
H_{min} 公里(6)	4.029	4.502	4.140	2.231	3.522	2.775

Key: (1) Scheme; (2) Sidewise jettison; (3) Towed cones; (4) Drag brakes; (5) Second; (6) Kilometer.

For the drag brake scheme, if twice brake opening is adopted the axial overload can be significantly reduced. At Δt=1.0 second, the maximum overload can be reduced by 1/3, yet the deceleration is also reduced. For the towed cone scheme, the time for towing out the towed cone does not have much influence on overload, and this result is in full agree-

ment with the conclusion from Reference [7] on a recovered body with pointed cone. Calculations have shown that if the recovery altitude and proportion of jettisoned weight are reasonably designed, the demand for sufficient kinetic pressure to open the parachute can be satisfied. When an ordinary parachute is used, after the demands for H=2.5 kilometers and M_∞=1.0 are satisfied, the demand for touchdown velocity can then be satisfied.

In fact, it can be seen from Fig. 13 that, in terms of the drag coefficient for each scheme, it is difficult to conculde which one is better and which one is worse. But from the point of view of drag, the bottom diameter is another important factor. If the towed cones and drag brakes schemes are of aft jettison mass, it is structurally arranged that their bottom diameters are generally smaller than that of the sidewise jettison-drag cones scheme. For these two schemes, both their structural problems in the jettison weight area must be resolved. Moreover, the stability of towed cone and heat resistance problem of the drag brake are also the aerodynamic problems of these two scheme which must be resolved respectively. Meanwhile, since jettisoning weight and increasing drag of these two schemes are accomplished by two movements, the complexity of the control systems are increased. For the sidewise jettison-drag scheme, since jettisoning weight and increasing drag are accomplished simultaneously by one movement, the requirements for the control system are lowered. But this scheme must clearly understand the aerodynamic interference between the shell body and the recovered in order to prevent the two bodies from colliding and too much disturbance on the recovered body. If the reentry vehicle has a certain attack angle before the recovery,

or asymmentrical separation occurs, the problem will be more complicated.

VII. Conclusions And Suggestions

1. Although the flow pattern of the recovered body for each recovery scheme has its own features, open type separation flow could occur in each case. If open type separation flow is present on the recovered body, the drag coefficient will be reduced significantly; therefore, the design should try as hard as possible to keep this kind of flow from occurring.

2. The drag coefficients for all the schemes decrease as M number increases under supersonic conditions, with the drag coefficients for the drag brake scheme decreasing at a slower pace. The bluntness ratio of the recovered body has significant incluence on the drag coefficient for every scheme. The change of corrosive combustion shape at the tip also has certain influences.

3. The ballistic analysis has shown that similar deceleration effects can be accomplished by every scheme. When selecting scheme, the advantages and disadvantages of each scheme in areas of aerodynamics, structure, heat resistance, control, requirements for the parachute, etc. must be weighed before making a decision. The aerodynamic interference problems in the weight jettisoning process of each scheme still require further study.

4. The results of wind tunnel tests on drag, pressure and heat and free flight ballistic target tests along with the engineering calculation data can be used, after they have been jointly analyzed, as the guidelines for preliminary design. In order to obtain more reliable aerodynamic data, the experimental techniques of existing devices still need improvements and the engineering calculation methods perfection. The nonviscous and viscous data calculation methods for complicated shapes must be studied, and in the meantime conditions must be created in order to conduct model free flight experiments.

The analytical calculations in this paper were completed by comrades Zhang XiaoLi and Xue Liming. In the process of completing this paper, supports were received from the Ministry of Aeronautical Industry, China Aerodynamic Research and Development Center, Benjing Institute of Aerodynamics and Institute of Mechanics of the Academia Sinica. Comrades Sun Yijuen, Zai Jingshe, Wen Yongyuan, Sun Hongshen, Zao Wenxiang and Wang Jianli gave much assistance. We hereby express our special thanks to all of them.

REFERENCES

[1] Rigali, D.J, and sterk, W.W., AIAA 80-1455 (1980).
[2] English, E. A., SAND 76-8009 (1976).
[3] Smith, D. H., AD-A066[illegible] (1978).
[4] Smith, D. H., AD-A066217 (1978).
[5] Charczenko, N. and Mosher, J. T., NASA TN D-9[illegible].
[6] Charczenko, N., NASA TN D-1799.
[7] Sims, L. W., *J. Spacecraft*, 8, 5(1971), 538—541.
[8] Steck, H. T., *J.Spacecraft*, 4, 6(1908), 716—750.
[9] Platus, D. H., *J. Spacecraft*, 13, 3 (1976), 270—251.
[10] Platus, D. H., AIAA 80-1571 (1980).
[11] 黄志澄, [illegible], 4(1984), 10—16.
[12] Charwat, A. F., et al, *J. Aerospace/sciences*, 28, 7(1961), 513—503.
[13] [illegible], (1982).
[14] [illegible], (1982).

[15] 杨跃栋，王复，郭大华：[illegible]，内部报告（1983）。
[16] 张晓清：回收方案估算和[illegible]，内部报告（1982）。
[17] 董文模：组合体模型[illegible]，内部报告（1982）。
[18] Ericsson, L. E.: AIAA 81-0070 (1981).
[19] 拖锥跨超声速风洞测力试验，内部报告（1982）。
[20] 周从直：拖锥高超声速风洞测力试验，内部报告（1982）。
[21] 陈　谦：拖锥方案测力试验，内部报告（1982）。
[22] 曹文祥：尾流流场及锥型方工程计算方法，内部报告（1982）。
[23] Lin, T. C., et al.: AIAA 79-1573 (1979).
[24] Cambell, J. and Grow, J. W.: NASA TN D-5389.
[25] Peterson, C. W. and Johnson, D. W.: AIAA 81-1939(1981).
[26] Moore, F. G.,DeJarnette, D. W. and Brooks, E. N. Jr.: AIAA 70-1176 (1970).
[27] Reding, J. P. and Ericsson, L. E.: *J. Spacecraft*, 4, 7(1967), 511-518.
[28] 夏　濂：回收体阻力板方案测力试验，内部报告(1982)。
[29] 杨跃栋，王复，郭大华：带有阻力板的回收模型在$M_\infty=7.8$时的阻力测量，内部报告(1982)。
[30] 温浦源：带分离控制板钝锥气动特性的工程计算方法，气动力学杂志，1(1984)，49—53。
[31] Berman, R., et. al: *J. Spacecraft*, 14, 3(1977), 163—169.
[32] 高瑞鲸：控制高超音速流场及压力特性实验研究，空气动力学学报，4(1984)，56—60。
[33] 韩宾达：阻力板局部线性实验研究，内部报告（1982）。
[34] 王基荫：攻角控制回收方案估计，内部报告（1982）。
[35] 可代云，蔡金芳：拖锥回收体动力学特性计算，内部报告（1982）。

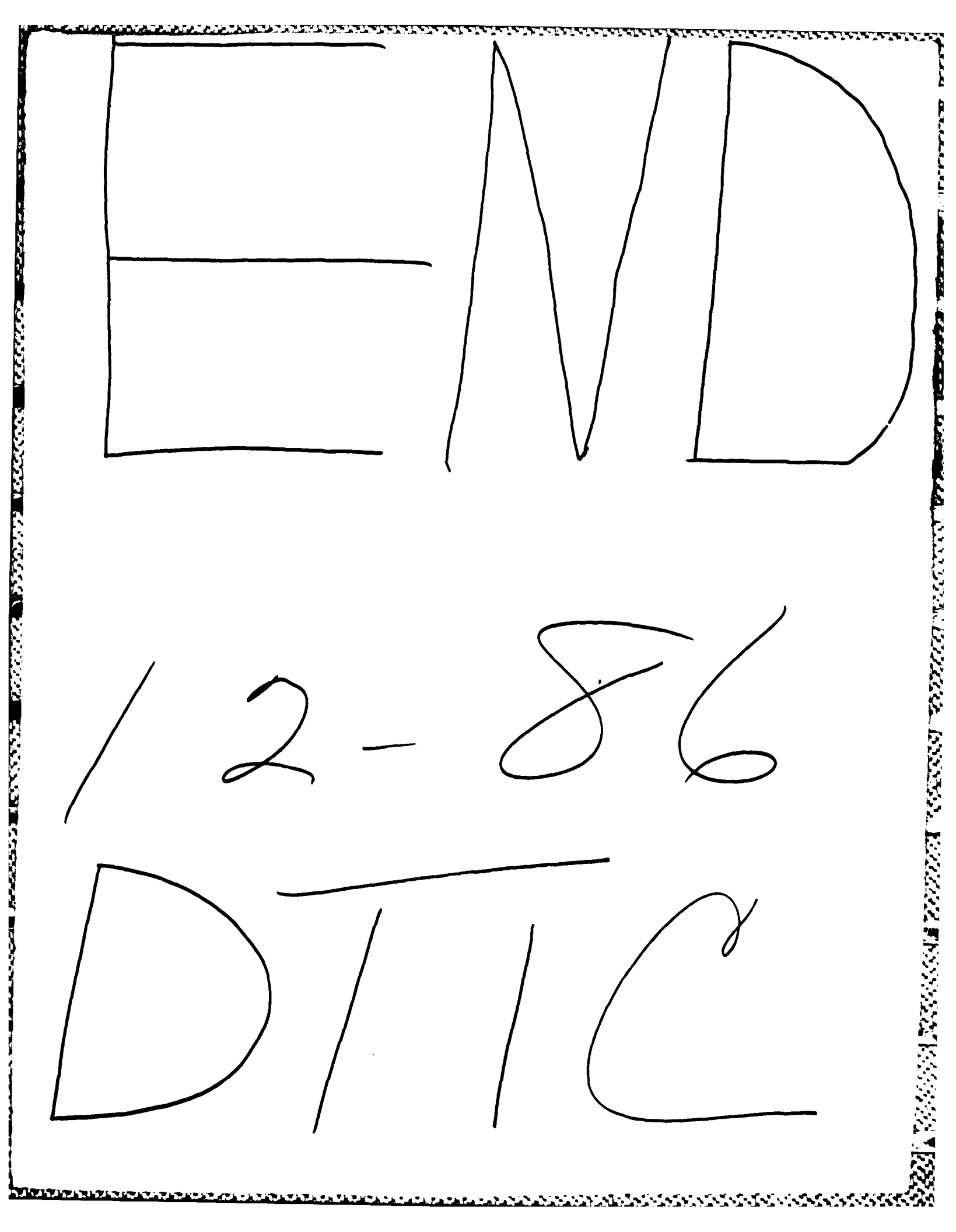
END
12-86
DTIC